JACS
JOURNAL OF THE AMERICAN CHEMICAL SOCIETY

Communication

pubs.acs.org/JACS

Regioselective Atomic Layer Deposition in Metal–Organic Frameworks Directed by Dispersion Interactions

Leighanne C. Gallington,[†] In Soo Kim,[‡] Wei-Guang Liu,[§] Andrey A. Yakovenko,[†] Ana E. Platero-Prats,[†] Zhanyong Li,[∥] Timothy C. Wang,[∥] Joseph T. Hupp,[∥] Omar K. Farha,[∥,⊥] Donald G. Truhlar,[§] Alex B. F. Martinson,[‡] and Karena W. Chapman*[,†]

[†]X-ray Science Division, Advanced Photon Source, Argonne National Laboratory, Argonne, Illinois 60439-4858, United States

[‡]Materials Science Division, Argonne National Laboratory, Argonne, Illinois 60439, United States

[§]Department of Chemistry, Chemical Theory Center, and Supercomputing Institute, University of Minnesota, Minneapolis, Minnesota 55455-0431, United States

[∥]Department of Chemistry, Northwestern University, Evanston, Illinois 60208-3113, United States

[⊥]Department of Chemistry, Faculty of Science, King Abdulaziz University, Jeddah 21589, Saudi Arabia

Supporting Information

ABSTRACT: The application of atomic layer deposition (ALD) to metal–organic frameworks (MOFs) offers a promising new approach to synthesize designer functional materials with atomic precision. While ALD on flat substrates is well established, the complexity of the pore architecture and surface chemistry in MOFs present new challenges. Through *in situ* synchrotron X-ray powder diffraction, we visualize how the deposited atoms are localized and redistribute within the MOF during ALD. We demonstrate that the ALD is regioselective, with preferential deposition of oxy-Zn(II) species within the small pores of NU-1000. Complementary density functional calculations indicate that this startling regioselectivity is driven by dispersion interactions associated with the preferential adsorption sites for the organometallic precursors prior to reaction.

Atomic layer deposition (ALD) is a versatile synthetic tool for atomically precise materials growth based on well-defined surface chemistries. ALD alternately delivers two complementary gaseous reagents to a substrate surface in sequential, self-limiting reactions,[1,2] and it has been widely applied to thin-film growth on locally flat surfaces[1−3] More recently, ALD has been extended to functionalize the three-dimensional internal surface of metal–organic frameworks (MOFs).[4,5] ALD in MOFs (or AIM) offers new routes to tune their surface chemistry for selective guest sorption and to produce designer catalysts.[4] The large aspect ratios of MOF pores, the heterogeneity of the pore surface (with inorganic and organic regions), and the complex pore architecture (with locally nonplanar surfaces) present new challenges for ALD. The influence of the MOF architecture on ALD reactions must be understood before we can control the structure and, thereby, the function of the resulting surface.

AIM has been widely explored for NU-1000, a zirconium-based MOF.[4] Its robust Zr_6O_8-based nodes impart high thermal and chemical stability,[6] allowing the structure to withstand the elevated temperatures and reactive gases utilized in ALD, and its open pores permit transport of the large organometallic ALD precursors.[4] AIM has been used to deposit various metal oxides and sulfides within NU-1000,[4,7−10] enabling catalysis of diverse reactions.[8,9,11]

The NU-1000 framework (Figure 1) has large hexagonal channels (~30 Å diameter) and triangular channels (~10 Å diameter) parallel to the *c* direction. Small pores (~8 Å) connect adjacent channels. The framework is formed by $Zr_6(O)_4(\mu\text{-OH})_4$ nodes connected via pyrene-based tetracarboxylate ligands.[4] Each node is coordinated by eight carboxylate donors, with terminal $-OH_x$ groups around the equator of the nodes providing surface sites for reaction with ALD precursors. While the $-OH_x$ groups are chemically equivalent, pairs of these reactive $-OH_x$ groups are alternately directed into either hexagonal channels or small pores.[12]

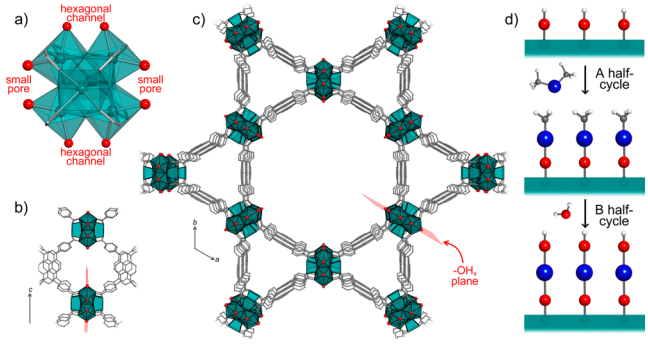

Figure 1. (a) Zr_6-based node (teal) in NU-1000 with pairs of $-OH_x$ ligands (red) directed into (b) the small pore and (c) hexagonal channels. (d) Schematic of an ALD reaction.

The uniform distribution of reactive $-OH_x$ groups around each node may be expected to yield uniform ALD, but our recent observations suggest that species are preferentially deposited in some pores. While diffusion (and, accordingly,

Received: August 19, 2016
Published: October 3, 2016

DOI: 10.1021/jacs.6b08711
J. Am. Chem. Soc. 2016, 138, 13513−13516

reaction) of the organometallic precursor through the large hexagonal channels is presumably most favorable,[4] new electron density following ALD treatment is observed in the small pores for the wide range of different ALD chemistries studied to date. This selective deposition on only half the node faces raises important questions about the mechanisms and energetics of the ALD processes.

Here we combine *in situ* synchrotron powder diffraction experiments and density functional calculations to explore these. We focus on Zn deposition using a diethylzinc (DEZ) precursor;[4] however, other ALD chemistries yield similar distributions and may be expected to follow similar reaction pathways. Differential analysis of structure envelopes (surfaces separating regions of high and low electron density[13,14]) yields coarse maps of the electron density associated with the deposited oxy-Zn(II) species. These analyses resolve whether the organometallic precursor preferentially reacts at certain $-OH_x$ sites and whether energy released by the precursor's decomposition redistributes species.

Powder X-ray diffraction data suitable for difference envelope density (DED) analysis were collected at beamline 17-BM (λ = 0.72768 Å). NU-1000 was diluted with SiO_2 powder (~1:1) to mimic its dispersal within in a standard ALD reactor and then loaded into a capillary assembled into a flow cell reactor.[15] Powder diffraction data were collected and analyzed as detailed in the Supporting Information, following progressive dosing of (A) DEZ vapor and (B) water vapor at 125 °C. Four (A+B) ALD cycles were monitored. Structure envelopes were calculated[16,17] using 24 reflections (to {6 −1 0}, h_{max}, k_{max}, $l_{max} \geq 2$), subtracting the envelope for NU-1000 at 125 °C to produce the DED.

The diffraction peak positions and intensities evolve during reaction of both the DEZ and H_2O vapors (Figure 2). These

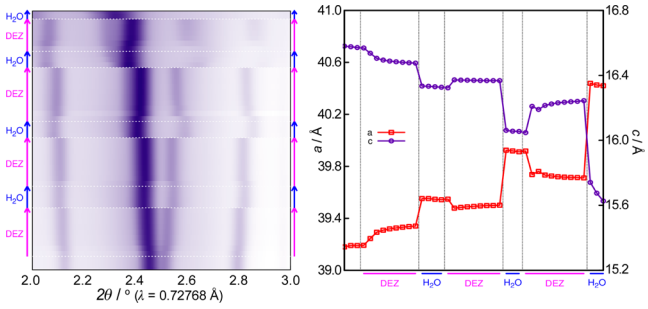

Figure 2. (Left) Powder X-ray diffraction data for NU-1000 during *in situ* ALD and (right) the corresponding lattice dimensions.

reflect changes to the NU-1000 lattice dimensions and electron density distribution, respectively. For each half-cycle, dosing was continued until minimal further changes to the diffraction data were evident. During DEZ (A) half-cycles these changes were gradual; during H_2O (B) half-cycles they were more abrupt, likely reflecting different diffusion rates for these species. Peak broadening, apparent following multiple ALD cycles, reflects increasing lattice disorder.

The changes to the NU-1000 lattice parameters induced by the ALD reactions, quantified through Le Bail analysis (Figure 2), reveal expansion in the *ab*-plane and contraction along the *c* axis, opposite to changes for a thermally induced distortion of the Zr_6-based nodes.[18]

During the first (A) half-cycle, DED analysis (Figure 3 and supplemental video) reveals new electron density localized on

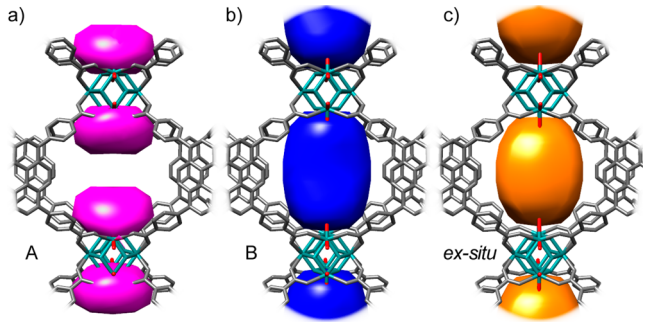

Figure 3. Difference envelope densities from *in situ* ALD during (a) the (A) half-cycle and (b) the (B) half-cycle, and (c) Zn-AIM prepared *ex situ*, focusing on the small pore of NU-1000.

the nodes, exclusively on node faces within the small pores, with no evidence of additional electron density on node faces within the large hexagonal channels. The electron density on the two nodes within each small pore is separated by a region of low electron density. Following subsequent exposure to water vapor during the (B) half-cycle, electron density on individual nodes within the small pores redistributes to bridge the nodes. The electron density distribution following a complete (A+B) cycle yields a picture that matches that of Zn-AIM prepared *ex situ*.

Subsequent ALD cycles show similar trends (Supporting Information and supplemental video). A second DEZ half-cycle added electron density in the small pore, localized close to the nodes; this density was redistributed to be centered in the small pores following the water half-cycle. A third DEZ half-cycle again added electron density in the small pore, localized close to the nodes, with a minor amount in the hexagonal channel; all electron density was redistributed to be centered in the small pores following the water half-cycle.

Several observations suggest that, in the present *in situ* study, DEZ dosing did not attain saturation as in *ex situ* synthesis. The lattice changes for Zn-AIM prepared *ex situ* match those seen here over multiple cycles. The lattice retains a greater degree of crystallinity than seen *ex situ*. Inductively coupled plasma–optical emission spectroscopy of the recovered material indicated that about eight Zn/Zr_6-based nodes were deposited after four ALD cycles, which includes an unknown amount of ZnO deposited on intermixed SiO_2 powder; four Zn per node can be deposited in a single conventional ALD cycle.

Kohn–Sham density functional theory was used to calculate the potential energies for the following steps in the deposition (TS is the transition state),

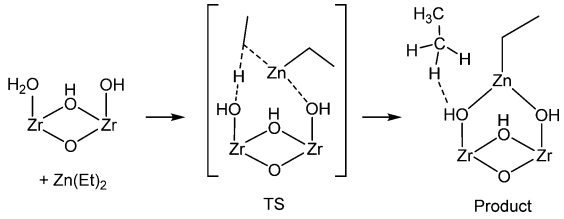

and the results are summarized in Table 1, in which calculations are presented with three different exchange-correlation functionals. A geometry-optimized model for NU-1000 was derived from the reported crystal structure[4] using the PBE-D2 or M06-L functional within CRYSTAL14.[19] In the optimization, the 6-31G(d)[20] basis set was used for H, C, and O, and the SDD effective core potential and corresponding basis set were used for Zr[21,22] and Zn,[23] with exponents less than 0.06 removed.

DOI: 10.1021/jacs.6b08711
J. Am. Chem. Soc. 2016, 138, 13513–13516

Table 1. Calculated Energies (kcal/mol) of DEZ Addition

	large channel		small pore		difference	
	TS	product	TS	product	TS	product
M06-L	−5.1	−53.2	−7.8	−54.4	−2.7	−1.2
PBE-D2	−10.6	−49.7	−13.7	−51.2	−3.1	−1.5
PBE//PBE-D2	3.1	−32.8	3.6	−32.2	+0.4	+0.6

For the resulting optimized geometry, the final energy was calculated by applying larger basis sets to fragments involved in the reaction (6-311++G** for C and H in DEZ, for the transferred H, and for the two O atoms that bond to Zn in the product), and diffuse functions on Zn discarded in the optimization were added back. The exponent of the diffusive basis was changed to 0.06 if smaller than 0.06.

The most reliable calculation is obtained with the M06-L[17] functional, which has been validated for bond energies and noncovalent interactions at van der Waals distances.[18] This functional provides reasonable predictions of damped dispersion at van der Waals distances but does not include the long-range component. The PBE-D2 functional combines the PBE functional[19] and the D2 molecular mechanics term[20] to account for dispersion. The D2 term is an atom-pairwise sum of damped r^{-6} functions, where r is an atom−atom distance. This term includes the long-range component of dispersion and damped dispersion at van der Waals distances.

Table 1 shows that the M06-L and PBE-D2 functionals, which both include dispersion effects, predict a lower energy for the transition state (TS) and (A) half-cycle product in the small pore relative to the large channel, in agreement with experiment. This explains the faster local deposition rate in the small pore and validates PBE-D2 for this problem, which allows a physical interpretation of the interaction energy differences in the two pores by recalculating the energy with just the PBE term. This calculation is denoted PBE//PBE-D2 to denote that the PBE-only calculation was carried out at the geometry optimized with PBE-D2. The lower energy for binding in the small pore is found only when dispersion is included.

To better understand the preferred binding in the small pore, the contributions to the D2 correction for dispersion were separated by partitioning atoms into three components: the ALD additive, the MOF ligand, and the node (Table 2). The preference for the small pore is dominated by additive−ligand interactions, whose sum is 3.3 and 2.3 kcal/mol larger in the small pore for the transition state and the product, respectively. Interactions between other components contribute less than 1.0 kcal/mol. The difference in D2 correction between the large channel and small pore is maximized at 4−5 Å; this indicates that, although the local coordination is equivalent in both pores, medium-range dispersion differentiates their energetics.

Table 2. Contributions to the Dispersion D2 Term (kcal/mol)[a]

	large channel		small pore		difference	
	TS	product	TS	product	TS	product
additive−linker	−4.9	−6.5	−8.1	−8.8	−3.3	−2.3
additive−node	−11.7	−13.5	−11.8	−12.4	+0.1	+1.0
additive−additive	−82.0	−5.7	−81.9	−6.4	+0.1	−0.7

[a]Additive includes Zn, C, H in Zn(Et) and ethane. Linker includes C, H in pyrene and benzoate. Node includes Zr, O, H in the node. There is no significant difference between the energies calculated for other pairs of components.

The present experiments demonstrate that the initial reaction of DEZ within NU-1000 occurs selectively on node faces within the small pores. This confirms that the selective deposition is associated with preferential reactivity at these sites and is not a consequence of relocation to the small pore during the B half-cycle.

Interestingly, some rearrangement of the deposited material occurs during the B half-cycle, whereby electron density that was localized on opposing nodes is redistributed to be centered between the nodes. This redistributed electron density bridges nodes along the c axis. It is accompanied by a substantial contraction of the lattice along this axis; the distance between nodes is reduced by ∼1 Å from ∼8.5 Å (O···O) in pristine NU-1000. We propose that, during the B half-cycle, species on opposing nodes within the same pore connect to form a Zn_xO_y cluster that draws the bridged nodes closer together, as reflected by a contraction of the c axis.

The density functional calculations suggest that dispersion interactions are implicated in the selective reaction within the small pores. The four benzoate ligands that form a cup around the node face within the small pore allow for greater dispersion interactions between organic ligands on the MOF surface and organics on the periphery of the organometallic reagent. By contrast, the node face within the more accessible hexagonal channel provides fewer dispersion interactions. For precursors such as DEZ, these dispersion effects outweigh any steric constraints. For larger ALD reagents, steric hindrance may become important.

The regioselectivity of ALD reactions can be understood by considering the preferential adsorption sites for the organometallic precursor. This recognizes that the precursor must be adsorbed as a guest within the MOF before it can react. Where guest−framework interactions are dominated by van der Waals rather than directional (e.g., hydrogen-bonding) interactions, the lowest energy adsorption sites are typically those that maximize contact with the guest. This interaction is maximized for pores that match to the size and shape of the adsorbate molecule—in this case, the small pores.

Adsorption and reaction are important, but separate, processes involved in AIM, with the interplay between the rates of reaction and transport (i.e., hopping between adsorption sites) influencing the result. While the ALD reagents are considered highly reactive, here, the reaction must occur on a slower time scale than transport between adsorption sites. The reagent molecule will spend more time in energetically favorable sites rather than moving between them. Molecular dynamics simulations are being pursued to explore how the precursor infiltrates the pores.

The importance of adsorption sites on the ALD process and resulting material is specific to MOFs. For ALD on locally flat surfaces (including larger mesopores) without favorable adsorption sites, uniform deposition is observed.

An interesting implication of the role of sorption and dispersion interactions is that this site selectivity could be modified or eliminated in condensed-phase reactions. In solution-based processes (e.g., for DEZ in toluene), the solvent can also be adsorbed within the MOF pores, with two possible effects. First, the more abundant solvent molecules may bind in the small pore and impede access by DEZ. Second, with solvent

DOI: 10.1021/jacs.6b08711
J. Am. Chem. Soc. 2016, 138, 13513−13516

molecules filling all pores, the dispersion interactions may be equalized.

In summary, we have uncovered an unsuspected regioselectivity for ALD in MOFs using *in situ* synchrotron X-ray scattering. The organometallic ALD reagent is only deposited at half of the available reaction sites. Counterintuitively, the deposition occurs not in the more accessible hexagonal channels, but instead in the small cavities that connect these channels. The surface functionalization achieved through AIM is modulated by the adsorption interaction of the organometallic precursor with the organic ligands of the MOF. This regioselectivity may be influenced by using precursors of different sizes. Ultimately, it is clear that the reaction and design rules for ALD in MOFs are far more complex than those of conventional ALD.

■ ASSOCIATED CONTENT

Supporting Information

The Supporting Information is available free of charge on the ACS Publications website at DOI: 10.1021/jacs.6b08711.

Details of X-ray experiments and analysis and computational modeling (PDF)

Video of evolving difference envelope densities during in situ AIM (AVI)

■ AUTHOR INFORMATION

Corresponding Author

*chapmank@aps.anl.gov

Notes

The authors declare the following competing financial interest(s): J.T.H. and O.K.F. have a financial interest in the start-up company NuMat Technologies, which is seeking to commercialize metal-organic frameworks.

■ ACKNOWLEDGMENTS

This work was supported as part of the Inorganometallic Catalysis Design Center, an Energy Frontier Research Center funded by the U.S. Department of Energy (DOE), Office of Science, Basic Energy Sciences, under Award No. DE-SC0012702. It used resources of the Advanced Photon Source, a U.S. DOE Office of Science User Facility operated for the DOE Office of Science by Argonne National Laboratory under Contract No. DE-AC02-06CH11357. A.E.P.-P. acknowledges a Beatriu de Pinós fellowship (BP-DGR 2014) from the Catalan Government.

■ REFERENCES

(1) Johnson, R. W.; Hultqvist, A.; Bent, S. F. *Mater. Today* **2014**, *17*, 236.

(2) George, S. M. *Chem. Rev.* **2010**, *110*, 111.

(3) Hamann, T. W.; Martinson, A. B. F.; Elam, J. W.; Pellin, M. J.; Hupp, J. T. *Adv. Mater.* **2008**, *20*, 1560.

(4) Mondloch, J. E.; Bury, W.; Fairen-Jimenez, D.; Kwon, S.; DeMarco, E. J.; Weston, M. H.; Sarjeant, A. A.; Nguyen, S. T.; Stair, P. C.; Snurr, R. Q.; et al. *J. Am. Chem. Soc.* **2013**, *135*, 10294.

(5) Leus, K.; Dendooven, J.; Tahir, N.; Ramachandran, R.; Meledina, M.; Turner, S.; Van Tendeloo, G.; Goeman, J.; Van der Eycken, J.; Detavernier, C.; et al. *Nanomaterials* **2016**, *6*, 45.

(6) Howarth, A. J.; Liu, Y.; Li, P.; Li, Z.; Wang, T. C.; Hupp, J. T.; Farha, O. K. *Nat. Rev. Mats.* **2016**, *1*, 15018.

(7) Kim, I. S.; Borycz, J.; Platero-Prats, A. E.; Tussupbayev, S.; Wang, T. C.; Farha, O. K.; Hupp, J. T.; Gagliardi, L.; Chapman, K. W.; Cramer, C. J.; Martinson, A. B. F. *Chem. Mater.* **2015**, *27*, 4772.

(8) Peters, A. W.; Li, Z.; Farha, O. K.; Hupp, J. T. *ACS Nano* **2015**, *9*, 8484.

(9) Li, Z.; Schweitzer, N. M.; League, A. B.; Bernales, V.; Peters, A. W.; Getsoian, A. B.; Wang, T. C.; Miller, J. T.; Vjunov, A.; Fulton, J. L.; et al. *J. Am. Chem. Soc.* **2016**, *138*, 1977.

(10) Klet, R. C.; Wang, T. C.; Fernandez, L. E.; Truhlar, D. G.; Hupp, J. T.; Farha, O. K. *Chem. Mater.* **2016**, *28*, 1213.

(11) Kung, C.-W.; Mondloch, J. E.; Wang, T. C.; Bury, W.; Hoffeditz, W.; Klahr, B. M.; Klet, R. C.; Pellin, M. J.; Farha, O. K.; Hupp, J. T. *ACS Appl. Mater. Interfaces* **2015**, *7*, 28223.

(12) Planas, N.; Mondloch, J. E.; Tussupbayev, S.; Borycz, J.; Gagliardi, L.; Hupp, J. T.; Farha, O. K.; Cramer, C. J. *J. Phys. Chem. Lett.* **2014**, *5*, 3716.

(13) McCusker, L. B.; Baerlocher, C.; Grosse-Kunstleve, R.; Brenner, S.; Wessels, T. *Chimia* **2001**, *55*, 497.

(14) Brenner, S.; McCusker, L. B.; Baerlocher, C. *J. Appl. Crystallogr.* **1997**, *30*, 1167.

(15) Chupas, P. J.; Chapman, K. W.; Kurtz, C.; Hanson, J. C.; Lee, P. L.; Grey, C. P. *J. Appl. Crystallogr.* **2008**, *41*, 822.

(16) Yakovenko, A. A.; Reibenspies, J. H.; Bhuvanesh, N.; Zhou, H.-C. *J. Appl. Crystallogr.* **2013**, *46*, 346.

(17) Yakovenko, A. A.; Wei, Z.; Wriedt, M.; Li, J.-R.; Halder, G. J.; Zhou, H.-C. *Cryst. Growth Des.* **2014**, *14*, 5397.

(18) Platero-Prats, A. E.; Mavrandonakis, A.; Gallington, L. C.; Liu, Y.; Hupp, J. T.; Farha, O. K.; Cramer, C. J.; Chapman, K. W. *J. Am. Chem. Soc.* **2016**, *138*, 4178.

(19) Dovesi, R.; Orlando, R.; Erba, A.; Zicovich-Wilson, C. M.; Civalleri, B.; Casassa, S.; Maschio, L.; Ferrabone, M.; De La Pierre, M.; D'Arco, P.; et al. *Int. J. Quantum Chem.* **2014**, *114*, 1287.

(20) Hehre, W. J.; Ditchfie, R.; Pople, J. A. *J. Chem. Phys.* **1972**, *56*, 2257.

(21) Andrae, D.; Häußermann, U.; Dolg, M.; Stoll, H.; Preuß, H. *Theor. Chim. Acta* **1990**, *77*, 123.

(22) Martin, J. M. L.; Sundermann, A. *J. Chem. Phys.* **2001**, *114*, 3408.

(23) Dolg, M.; Wedig, U.; Stoll, H.; Preuss, H. *J. Chem. Phys.* **1987**, *86*, 866.

DOI: 10.1021/jacs.6b08711
J. Am. Chem. Soc. 2016, 138, 13513−13516